Monatsh Chem (2011) 142:97–109
DOI 10.1007/s00706-010-0409-y

ORIGINAL PAPER

Exploring the molecular basis for selective cytotoxicity of lamellarins against human hormone-dependent T47D and hormone-independent MDA-MB-231 breast cancer cells

Poonsiri Thipnate · Montakarn Chittchang · Nopporn Thasana · Patchreenart Saparpakorn · Poonsakdi Ploypradith · Supa Hannongbua

Received: 5 May 2010 / Accepted: 7 August 2010 / Published online: 5 November 2010

Abstract The common structural requirements for cytotoxicity of lamellarins against two human breast cancer cell lines were determined using comparative molecular field analysis (CoMFA) and comparative molecular similarity indices analysis (CoMSIA) techniques. Twenty lamellarins were selected to serve as the training set, whereas another group of six compounds were used as the test set. The best CoMFA and CoMSIA models for both cell lines yielded satisfactory predictive ability with r^2_{cv} values in the range of 0.659–0.728. Additionally, the contour maps obtained from both the CoMFA and CoMSIA models agreed well with the experimental results and may be used in the design of more potent cytotoxic compounds for human breast cancers. Both analyses not only suggested structural requirements of various substituents around the lamellarin skeleton for their cytotoxic activity against both human breast cancer cell lines but also revealed the molecular basis for the differences between the saturated and unsaturated D-rings of the lamellarins.

Keywords QSAR · CoMFA · CoMSIA · Lamellarins · Human breast cancer · Cytotoxicity

P. Thipnate · P. Saparpakorn · S. Hannongbua (✉)
Department of Chemistry, Faculty of Science, Kasetsart University (KU), Chatuchak, Bangkok 10900, Thailand
e-mail: fscisph@ku.ac.th

P. Thipnate · P. Saparpakorn · S. Hannongbua
Center of Nanotechnology, Kasetsart University (KU), Chatuchak, Bangkok 10900, Thailand

M. Chittchang · N. Thasana · P. Ploypradith
Chulabhorn Research Institute and Chulabhorn Graduate Institute, Vibhavadee-Rangsit Highway, Laksi, Bangkok 10210, Thailand

Introduction

Lamellarins (Fig. 1) are marine-derived polyaromatic pyrrole alkaloids that have been isolated from different sources, such as ascidians, molluscs, and sponges [1–11]. To date, more than 30 lamellarins have been isolated, many of which exhibit interesting biological activities. For example, lamellarin α 20-sulfate is a potential candidate for human immune-deficiency virus (HIV) treatments as it can inhibit HIV-1 integrase in vitro [12, 13]. On the other hand, nonsulfated lamellarins appear to possess potent cytotoxic activity against cancer cells [14], especially lamellarin D, which has been receiving a lot more attention than all the other compounds in this series. Their cancer cytotoxicity has been attributed to the finding that lamellarin D is an effective stabilizer of human topoisomerase I–DNA covalent complexes, and thus capable of stimulating DNA cleavage [15, 16]. More recently, lamellarin D has also been demonstrated to induce apoptosis as well as to disrupt the inner transmembrane potential of mitochondria, which is a novel pharmacological target for anticancer chemotherapy [17–21]. Additionally, lamellarin D and some other lamellarins have shown potent inhibition of various protein kinases [22]. Nontoxic doses of some lamellarins, especially lamellarin I, can also reverse multidrug resistance (MDR) of cancer cells by inhibiting P-glycoprotein (P-gp)-mediated drug efflux with a 9–16 times higher MDR modulating potency than that of verapamil [23].

Even though lamellarins D, K, and M are usually classified among the most cytotoxic molecules in the lamellarin series, structure–activity relationship studies of lamellarins for their cytotoxicity towards cancer cell lines have exclusively focused on lamellarin D and its derivatives. Generally, lamellarins with a C5–C6 double bond are more

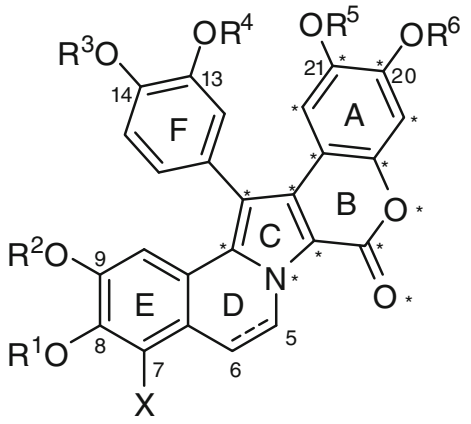

Fig. 1 Core structure of the lamellarins, in which the common atoms used for three-dimensional (3D) quantitative structure–activity relationship (QSAR) matching alignments are denoted by *asterisks*

cytotoxic than those bearing a C5–C6 single bond. However, some exceptions have been observed with lamellarin M, which is roughly equally cytotoxic to its saturated counterpart, lamellarin K, whereas lamellarin M-triacetate is actually much less cytotoxic than its corresponding analogue in the saturated series, lamellarin K-triacetate [23, 24]. For the substituents on the lamellarin core, it appears that the hydroxyl groups at the C8 and C20 positions of lamellarin D are important structural requirements, while the hydroxyl group at C14 and the two methoxy groups at C13 and C21 are not necessary for cytotoxic activity [25, 26]. Employing a systematic approach based on a large number of lamellarins and cancer cell lines, our recent findings not only substantiate the significant contributions of the C5–C6 olefin moiety as well as the hydroxyl groups at C8 and C20, but also demonstrate the importance of the C7 hydroxyl group for the first time [29].

Computational chemistry has been used to verify and explain these experimental findings. Molecular models of the ternary complex formed between topoisomerase I–DNA with a lamellarin D molecule fully intercalating into the DNA duplex have been created using the AutoDock 3.0 docking program and studied using nanosecond molecular dynamics simulations in aqueous solution [15, 26]. The results confirm that the C8 and C20 hydroxyl groups on the lamellarin core are the major determinants of both the topoisomerase I cleavable complex stabilization and the cytotoxic action. In contrast, there is no clear explanation for the functional role of the C5–C6 double bond, which when present in the quinoline D-ring tends to make the compounds more cytotoxic than those having a C5–C6 single bond. In more recent findings, a small number of structurally different lamellarins have been successfully used to generate 3D pharmacophore mapping for the cytotoxicity of lamellarins against human hormone-dependent T47D breast cancer cell. Four-dimensional (4D) quantitative structure–activity relationship (QSAR) and 3D pharmacophore were built and investigated for this cytotoxicity using only 26 lamellarins [28]. However, no explanation for the difference between C5–C6 double and single bond was found in this work.

In our previous studies, these 26 natural and unnatural lamellarins were synthesized using our published synthetic routes [29] and tested for their cytotoxicity against 11 cancer cell lines [27]. The prominent selectivity observed with certain lamellarins towards human hormone-dependent T47D and hormone-independent MDA-MB-231 breast cancer cells has prompted us to further investigate the possible underlying reasons. With the inclusion of two unnatural compounds (dehydrolamellarins J and Y), a total of ten pairs of lamellarins, each of which only differ in the presence of either a saturated or an unsaturated D-ring (Tables 1, 2), were used to explore their potential differences in steric, electrostatic, hydrophobic, and hydrogen-bond interactions in detail.

The questions addressed in the present study are not only what causes the different cytotoxicity of saturated and unsaturated quinoline D-ring lamellarins, but also why lamellarins show different cytotoxicity in both breast cancer cells. Therefore, 3D-QSAR methods were employed to understand the mechanism of the interactions between ligands and an unknown receptor. In order to use these methods, the physicochemical properties of 26 lamellarin molecules were represented in the form of molecular fields, which could then be effectively correlated with their cytotoxic activity using partial least-squares (PLS) regression analysis [30–32]. Additionally, comparative molecular field analysis (CoMFA) [31] and comparative molecular similarity indices analysis (CoMSIA) [30, 32] techniques were applied to examine the molecular basis for the differences between the lamellarins containing a saturated D-ring and those with a C5–C6 double bond. The common structural requirements for their cytotoxic activity against both human breast cancer cell lines were also determined.

Results and discussion

Twenty-six lamellarins used in this study can be classified into two groups that differ mainly in the nature of the C5–C6 bond in the D-ring. Eleven compounds with a saturated D-ring in Table 1 (excluding lamellarin G and the acetate-containing derivatives) contain exactly the same substituents as their corresponding analogues with a C5–C6 double bond in Table 2, e.g., lamellarins C and B, lamellarins E and X, etc. Most of the compounds used in this study were naturally occurring lamellarins, except the two unnatural

Table 1 Structure and cytotoxic activity of lamellarins with a saturated D-ring

Lamellarin	Substituent group							$-\log IC_{50}$	
	X	OR^1	OR^2	OR^3	OR^4	OR^5	OR^6	T47D	MDA-MB-231
C	OMe	OMe	OMe	OH	OMe	OMe	OH	5.11	5.08
E	OH	OMe	OMe	OMe	OH	OMe	OH	5.28	5.47
F	OH	OMe	OMe	OMe	OMe	OMe	OH	5.34	5.44
G	H	OH	OMe	OMe	OH	OH	OMe	5.07	4.83
I	OMe	OMe	OMe	OMe	OMe	OMe	OH	5.02	5.07
J	H	OH	OMe	OMe	OMe	OMe	OH	4.89	5.13
K	OH	OMe	OMe	OH	OMe	OMe	OH	7.04	6.40
L	H	OH	OMe	OMe	OH	OMe	OH	5.36	5.75
T	OMe	OMe	OMe	OMe	OH	OMe	OH	4.88	5.06
U	H	OMe	OMe	OMe	OH	OMe	OH	4.99	5.35
Y	H	OMe	OH	OMe	OH	OMe	OH	5.14	4.10
χ	H	OH	OMe	OH	OMe	OMe	OH	5.42	5.32
K triacetate	OAc	OMe	OMe	OAc	OMe	OMe	OAc	5.18	5.33
U diacetate	H	OMe	OMe	OMe	OAc	OMe	OAc	5.10	5.46
χ triacetate	H	OAc	OMe	OAc	OMe	OMe	OAc	5.54	5.18

Table 2 Structure and cytotoxic activity of lamellarins with an unsaturated D-ring

Lamellarin	Substituent group							$-\log IC_{50}$	
	X	OR^1	OR^2	OR^3	OR^4	OR^5	OR^6	T47D	MDA-MB-231
B	OMe	OMe	OMe	OH	OMe	OMe	OH	6.74	5.35
D	H	OH	OMe	OH	OMe	OMe	OH	10.10	6.40
M	OH	OMe	OMe	OH	OMe	OMe	OH	8.02	6.95
N	H	OH	OMe	OMe	OH	OMe	OH	9.22	6.22
W	OMe	OMe	OMe	OMe	OH	OMe	OH	5.37	5.29
α	H	OMe	OMe	OMe	OH	OMe	OH	6.23	5.41
X	OH	OMe	OMe	OMe	OH	OMe	OH	8.25	7.12
ε	OH	OMe	OMe	OMe	OMe	OMe	OH	8.26	6.59
ζ	OMe	OMe	OMe	OMe	OMe	OMe	OH	7.05	5.33
Dehydrolamellarin J	H	OH	OMe	OMe	OMe	OMe	OH	10.01	6.41
Dehydrolamellarin Y	H	OMe	OH	OMe	OH	OMe	OH	7.10	6.19

dehydrolamellarins J and Y, as well as three acetate-containing derivatives, which were also included in order to investigate the effect of acetylation on the cytotoxic activity of lamellarins. After aligning all lamellarins by using matching alignment, their orientations are represented in Fig. 2. It was shown that the overall planarity of the fused ring system (A through E) could be achieved only in the lamellarins containing a C5–C6 double bond (unsaturated D-ring), while those with a C5–C6 single bond in the D-ring were not planar, as the substituents on the E-ring (e.g., C7, C8, and C9) were spatially displaced. All structures in Fig. 2 were used for calculations of CoMFA and CoMSIA analysis in further analysis.

The cytotoxicity of lamellarins containing either a saturated or an unsaturated D-ring against T47D and MDA-MB-231 human breast cancer cell lines are presented in Tables 1 and 2 as the negative logarithm of the 50% inhibition concentration (IC_{50}) values previously reported by Chittchang et al. [27] except those of the three acetate-containing compounds. Interestingly, lamellarins with a C5–C6 single bond exhibited comparable cytotoxic activity towards both cell lines, with IC_{50} values of the same order of magnitude (Table 1). On the other hand, it is clearly demonstrated in Table 2 that all of the compounds with an unsaturated D-ring were significantly more cytotoxic to the hormone-dependent T47D cell line. Overall, lamellarins D

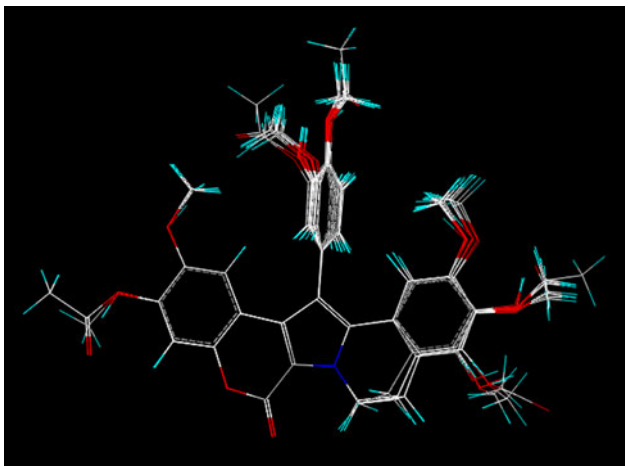

Fig. 2 Structure of lamellarins, obtained from 3D-QSAR matching alignments

and X were the most potent cytotoxic compounds against the T47D and MDA-MB-231 cell lines, respectively.

CoMFA and CoMSIA for cytotoxicity of lamellarins against T47D cells

CoMFA and CoMSIA models

Table 3 summarizes various parameters associated with the CoMFA models obtained by calculating the steric and electrostatic interactions between the aligned lamellarin molecules with each probe atom, which were subsequently correlated with their cytotoxic activity to identify the important interactions determining the cytotoxicity of lamellarins. All the models indicated that the changes in the steric interactions accounted for approximately two-thirds of the changes in the cytotoxic activity of lamellarins towards T47D cells, and the remaining 33–34% was contributed by the electrostatic interactions. Among the three CoMFA models for the T47D cell line, namely models 1–3 in Table 3, model 1, calculated using a sp^3 carbon as the probe atom, yielded the highest predictive ability, as indicated by the r^2_{cv} (or q^2) value. However, based on the F value and the $r^2_{test\ set}$, model 2 appeared to be the best CoMFA model of the T47D cell line. Other statistical parameters were comparable among the three models.

To further explore whether other types of interactions also play an important role in determining the cytotoxic activity of lamellarins in both cell lines, CoMSIA was also performed, and five models were generated using different combinations of steric (St), electrostatic (El), hydrophobic (Hyd), H-bond donor (Hd), and H-bond acceptor (Ha) field types, as shown in Table 4. However, only models 7 and 8 yielded acceptable predictive ability, as indicated by r^2_{cv} values of >0.6. Additionally, whenever the hydrogen-bond donor and/or acceptor fields were included, i.e., models 9–13, the r^2_{cv} values were significantly decreased. These findings suggest that only the steric, electrostatic, and hydrophobic fields are important for the predictive ability of the model derived for breast cancer cell lines.

Model 8 was derived from model 7 upon the exclusion of lamellarin J with the lowest activity in the training set, resulting in a model with improved r^2_{cv} as well as a lower standard error of estimation (s). Hence, model 8 was selected as the best CoMSIA model for T47D cells. All the CoMSIA models indicated that steric interactions accounted for approximately <12% of the changes in the cytotoxic activity of lamellarins, whereas the major contributions actually came from the electrostatic and hydrophobic fields.

The predictive ability of the selected CoMFA and CoMSIA models was determined using six lamellarin compounds as the test set. The CoMFA model was first considered, and the $-\log IC_{50}$ values predicted using

Table 3 Summary of CoMFA results for T47D and MDA-MB-231 cell lines

Model[a]	Probe atom	noc[b]	r^2_{cv} [c]	S-PRESS[d]	r^2 [e]	s[f]	F[g]	Steric contribution	$r^2_{test\ set}$
1	sp^3 C(+1)	6	0.717	1.143	0.963	0.414	56.144	66.0	0.466
2	sp^3 O(+1)	6	0.659	1.255	0.965	0.405	58.959	66.9	0.628
3	H(+1)	6	0.672	1.231	0.965	0.403	59.581	66.7	0.570
4	sp^3 C(+1)	6	0.661	0.498	0.977	0.129	92.967	67.6	0.408
5	sp^3 O(+1)	6	0.728	0.447	0.981	0.117	114.66	68.1	0.364
6	H(+1)	6	0.685	0.481	0.974	0.138	81.624	66.3	0.405

[a] Model 1–3 for T47D cell line and model 4–6 for MDA-MB-231 cell line

[b] The optimum number of components

[c] Cross-validated correlation coefficient

[d] Uncertainty of the prediction

[e] Conventional correlation coefficient

[f] Standard error of estimation

[g] F value

Table 4 Summary of CoMSIA results for T47D and MDA-MB-231 cell lines

Model[a]	Field type	noc.[b]	r^2_{cv}	S-PRESS	r^2	s	F	Contributions	$r^2_{test\ set}$
7	St + El + Hyd	5	0.623	1.271	0.923	0.575	33.541	St = 11.8 El = 45.7 Hyd = 42.5	0.918
8[c]	St + El + Hyd	6	0.662	1.271	0.960	0.436	48.321	St = 11.6 El = 45.8 Hyd = 42.6	0.894
9	St + El + Hd	1	−0.090	1.907	0.325	1.500	8.688	St = 0.059 El = 0.302 Hd = 0.639	–
10	St + El + Ha	1	−0.080	1.898	0.229	1.604	5.344	St = 0.082 El = 0.420 Ha = 0.498	–
11	St + El + Hyd + Hd	5	0.489	1.480	0.900	0.655	25.153	St = 5.0 El = 25.6 Hyd = 27.8 Hd = 41.6	–
12	St + El + Hyd + Ha	5	0.548	1.393	0.913	0.611	29.324	St = 8.0 El = 33.9 Hyd = 34.3 Ha = 23.8	–
13	All	5	0.429	1.565	0.885	0.703	21.497	St = 4.2 El = 21.8 Hyd = 25.5 Hd = 37.2 Ha = 11.3	–
14	St + El + Hyd	6	0.608	0.536	0.954	0.184	44.956	St = 10.5 El = 48.3 Hyd = 41.1	0.595
15[d]	St + El + Hyd	6	0.674	0.445	0.952	0.171	39.651	St = 10.2 El = 49.9 Hyd = 39.8	0.582
16	St + El + Hd	6	0.131	0.798	0.954	0.184	44.670	St = 0.058 El = 0.302 Hd = 0.633	–
17	St + El + Ha	1	−0.167	0.786	0.228	0.639	5.323	St = 0.077 El = 0.402 Ha = 0.521	–
18	St + El + Hyd + Hd	6	0.547	0.576	0.964	0.164	57.245	St = 5.0 El = 24.8 Hyd = 20.6 Hd = 49.6	–
19	St + El + Hyd + Ha	6	0.424	0.650	0.939	0.211	33.540	St = 7.6 El = 32.9 Hyd = 29.0 Ha = 30.6	–

Table 4 continued

Model[a]	Field type	noc.[b]	r^2_{cv}	S-PRESS	r^2	s	F	Contributions	$r^2_{test\ set}$
20	All	6	0.458	0.630	0.957	0.177	48.572	St = 4.1 El = 19.0 Hyd = 18.7 Hd = 44.4 Ha = 13.8	–

St steric; *El* electrostatic; *Hyd* hydrophobic, *Hd* H-bond donor; *Ha* H-bond acceptor

[a] Model 7–13 for T47D cell line and model 14–20 for MDA-MB-231 cell line

[b] The optimum number of components

[c] Elimination of lamellarin J

[d] Elimination of lamellarin Y

model 2 were plotted against the experimentally determined values (Fig. 3a). The prediction results were satisfactory for most of the compounds in the test set with the exception of lamellarin α. Exclusion of this compound from the test set significantly improved the $r^2_{test\ set}$ value for model 2 to 0.985. Similarly, the selected CoMSIA model 8 was also validated, and the results are presented in Fig. 3b. The model appeared to overestimate the $-\log IC_{50}$ values of lamellarin α and lamellarin M, while the predicted value of lamellarin K was lower than the experimental $-\log IC_{50}$ value. Nevertheless, CoMFA model 2 could be used to predict the cytotoxic activity of most lamellarins in the test set towards T47D cells.

CoMFA and CoMSIA contour maps

CoMFA and CoMSIA contour maps were created using the best CoMFA and CoMSIA models for each cell line, as shown in Figs. 4 and 5. The resulting contours on these maps not only highlight the key structural features correlated with the biological activity of the molecules considered but also provide detailed understanding of the binding pockets. Green and yellow regions represent areas where steric bulk enhanced and diminished biological activity, respectively. On the other hand, blue and red contours represent regions where electropositive and electronegative groups were associated with cytotoxicity, respectively. To avoid any ambiguity due to contour overlap, all contours are displayed in transparent style. Additionally, lamellarin D and lamellarin X, which were the most active molecules against T47D and MDA-MB-231 cell lines, respectively, were used as the reference molecules in the corresponding contour maps.

Interestingly, Fig. 4a clearly shows several steric and electrostatic contours generated using CoMFA model 2 for the T47D cell line. For the pentacyclic core, all contours were concentrated around the two rightmost D- and E-rings (Fig. 4a). There were green and blue regions near the C9 group. Red contours also occupy the space between the oxygen atom of the methoxy group at C9 and the hydroxyl group at C8. These suggest that oxygen atoms at C8 and C9 were important for cytotoxic activity. The steric and electropositive group at C9 might play an important role for activity. Considering two pairs of lamellarins (lamellarin Y compared with lamellarin U and dehydrolamellarin Y compared with lamellarin α), it was shown that the cytotoxic activity of the lamellarins was decreased when the C9 hydroxy group was replaced by a methoxyl group, which is somewhat different from the green contour of the predictive model. The reason for this is that both lamellarin U and lamellarin α were solely employed in the test set. Interesting contours in the E-ring were blue contours at the hydrogen atom and methyl group at C7, and a red contour located around the oxygen atom at C7. These might indicate that occupancy of the hydroxyl and methoxyl group was more cytotoxic than a hydrogen atom at this position. This result supports the pronouncement of Chittchang et al. [27] that substitution of the hydrogen atom at C7 with a hydroxyl group significantly increased the cytotoxicity of unsaturated lamellarins.

In terms of the orthogonal ring or F-ring, a large green contour was found virtually covering this ring. This finding suggests that the orthogonal ring of lamellarin could be essential for activity. Additionally, a red contour was found near an oxygen atom and an acetate group at C14 of the lamellarin. This contour showed that the oxygen atom and acetate group at C14 might be important for activity. The blue contour regions between C13 and C21 groups suggested that some electropositive groups in these areas might be advantageous for activity.

Finally, a yellow contour appeared behind the plane of the molecule near the C5–C6 double bond, while blue and green contours occupy the space around the D-ring. The yellow contour shows sterically unfavored areas near the C5–C6 double bond. This prediction, along with the superior cytotoxicity of the lamellarins containing a C5–C6

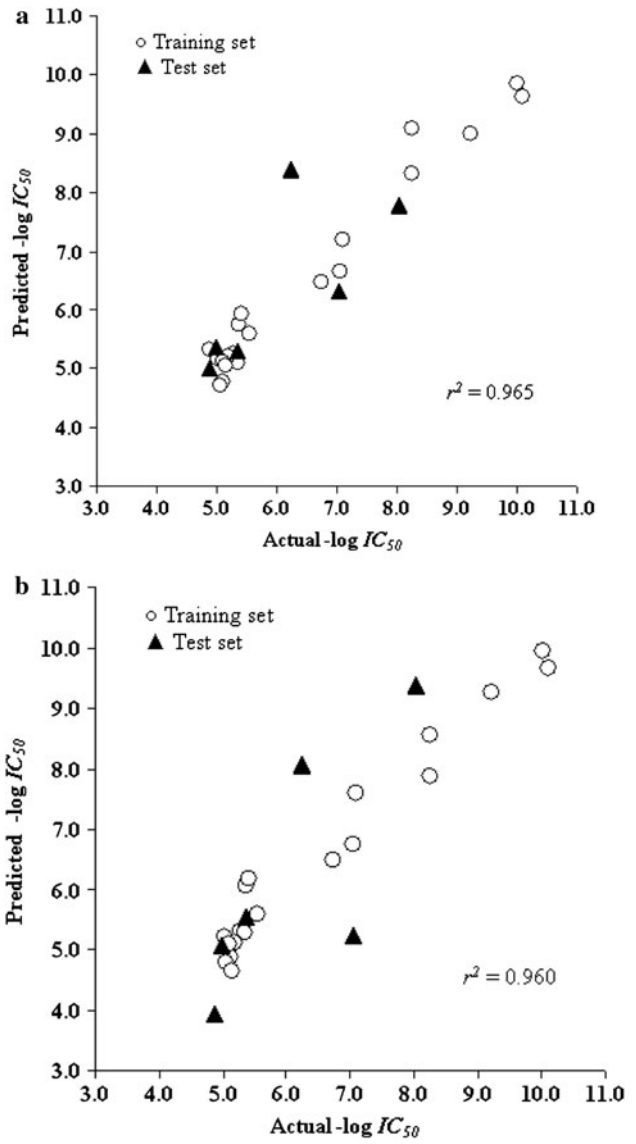

Fig. 3 Plot of predicted versus actual cytotoxic activity of lamellarins towards T47D cells. Predicted values were obtained from non-cross-validated CoMFA model 2 (**a**) and CoMSIA model 8 (**b**) for all compounds in both the training (*open circle*) and test (*filled triangle*) sets

double bond (Tables 1, 2), suggests that these compounds assume a structure that could fit into the binding pocket better than their counterparts with a single bond. It was observed in our preliminary molecular modeling studies that the lamellarins with a saturated D-ring were twisted, whereas the presence of the C5–C6 double bond leads to a more planar molecule that is likely to intercalate into the topoisomerase I–DNA complex more easily [27]. The blue and green contours result from the twisted bond of unsaturated lamellarins which cannot align at the same position as shown in Fig. 2.

In addition to the steric and electrostatic fields considered in CoMFA, CoMSIA helps to define the contribution of the explicit hydrophobic interactions to the binding affinity of lamellarins, as shown in Fig. 5. Orange and white contours indicate areas where the presence of hydrophobic groups is associated with increase and decrease of biological activity, respectively. Since CoMSIA steric and electrostatic contours were shown in more detail than those of the CoMFA models at some positions, all three field contributions are discussed. The steric and electrostatic contours from the best CoMSIA model for the T47D cell line are shown in Fig. 5a. There was a green region at C9 and a white region near the oxygen atom at C9. Both contours indicated that the oxygen atom at this position was essential for potent cytotoxic activity. The presence of steric (yellow contour near the hydrogen atom), electrostatic (blue contour near the hydrogen atom and methyl group, and red contour near the oxygen atom), and hydrophobic (white contour) fields at C8 revealed that a nonsteric electropositive group around this area was required for better activity. The suggestion has been reported by Ishibashi et al. [25] and Chittchang et al. [27] that a hydroxyl group at C8 of lamellarin D is an important structural requirement for activity.

Furthermore, yellow and green contours near the hydroxyl and methoxyl group at C7 led to the idea that a bulky group at this position would increase activity, but the size of this group should not be too large. Additionally, there was a blue region near the hydroxyl and methoxyl group at C7, a red region located around the oxygen atom at C7, and a white region at C7. These might indicate that a steric electron-donating oxygen-containing group such as hydroxyl or methoxyl group would be beneficial for cytotoxicity. These findings support the work of Chittchang et al. [27] that replacement of the hydroxyl group at C7 by a methoxy group decreases the cytotoxic activity of unsaturated lamellarins. More hydrophobic fields (white, orange, and red contours) were found around the C5–C6 bond. The white contour appeared at CH_2 around the C5–C6 bond. The orange and red contours were located around the C5–C6 bond. Both contours could not play any important role in activity. These fields were shown around this area because of the difference in planarity between the lamellarins containing C5–C6 single and double bond, which could not align into the same plane. These results also confirm that the structural requirement relied more on the double rather than the single bond. The red contours located between the oxygen atom of C13 and C14 positions and near the carbonyl of the acetate group around C20 revealed the importance of the oxygen atom at these areas for cytotoxicity. The two green regions located at C13 and C21 suggest that the substituents at these positions should be bulky groups.

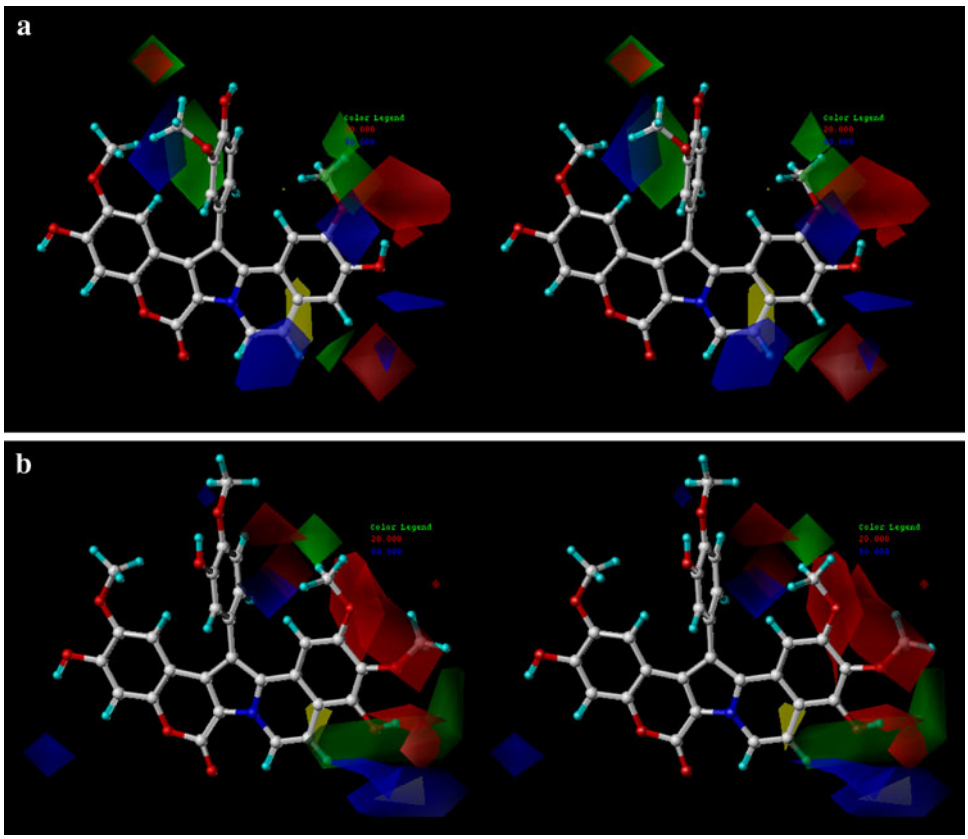

Fig. 4 Stereoviews of steric and electrostatic standard deviation × coefficient contour maps, obtained from CoMFA model 2 for T47D cytotoxicity (**a**) and CoMFA model 5 for MDA-MB-231 cytotoxicity (**b**). Lamellarins D and X are presented inside the fields of the T47D and MDA-MB-231 CoMFA contour maps, respectively, in ball-and-stick display style. Sterically favored and unfavored areas are shown by *green* and *yellow* regions, respectively. Electropositive and electronegative areas are shown by *blue* and *red* regions, respectively

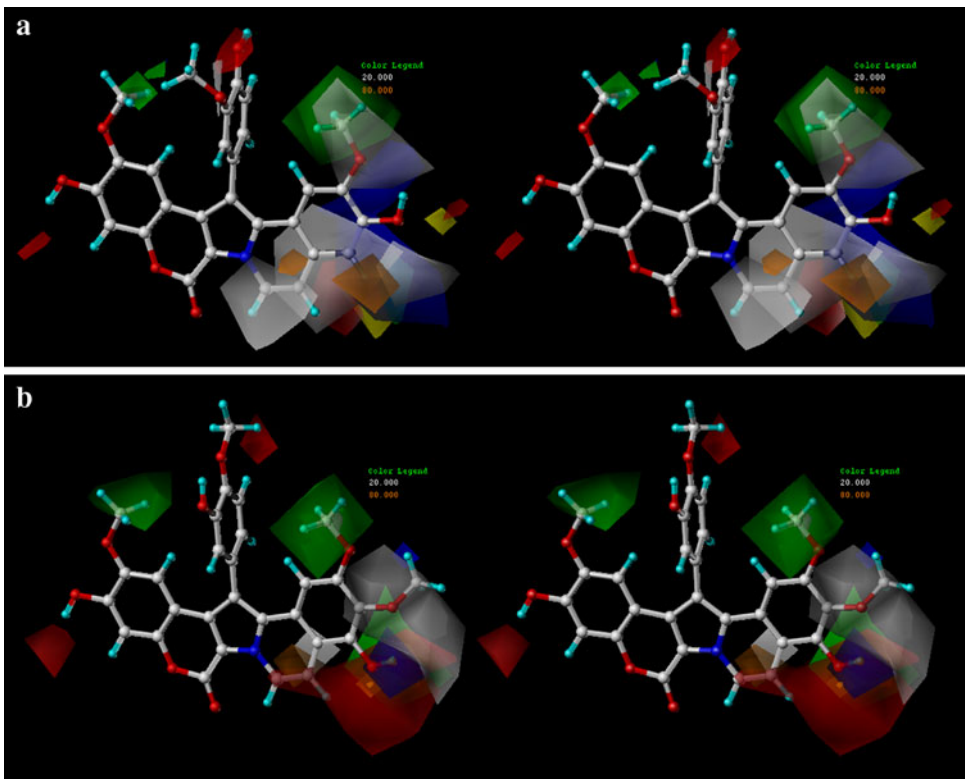

Fig. 5 Stereoviews of steric, electrostatic, and hydrophobic standard deviation × coefficient maps, obtained from CoMSIA model 8 for T47D cytotoxicity (**a**) and CoMSIA model 15 for MDA-MB-231 cytotoxicity (**b**). Lamellarins D and X are presented inside the fields of the T47D and MDA-MB-231 CoMFA contour maps, respectively, in ball-and-stick display style. Sterically favored and unfavored areas are shown by *green* and *yellow* regions, respectively. Electropositive and electronegative areas are shown by *blue* and *red* regions, respectively. Hydrophobically favored and unfavored areas are shown by *orange* and *white* regions, respectively

CoMFA and CoMSIA for the cytotoxicity of lamellarins against MDA-MB-231 cells

CoMFA and CoMSIA models

The CoMFA and CoMSIA models for the MDA-MB-231 cell line were generated using the same compounds in the training and test sets as those used for the T47D cell line. The statistical parameters associated with CoMFA models 4–6 for the MDA-MB-231 cell line are shown in Table 3. Apparently, model 5 obtained using an sp^3 oxygen as the probe atom yielded not only the highest predictive ability with an r^2_{cv} value of 0.728 but also the highest F value. Even though the other statistical parameters were not significantly different among the three models, model 5 still appeared to be the best CoMFA model for the MDA-MB-231 cell line, which indicated that steric interactions were the major factor, contributing approximately 68% of the changes in cytotoxic activity of lamellarins towards MDA-MB-231 cells.

With the sequential additions of the hydrophobic and hydrogen-bonding interactions, seven CoMSIA models (models 14–20) were subsequently constructed for the MDA-MB-231 cell line, as shown in Table 4. Based on the r^2_{cv} values, the models involving only the steric, electrostatic, and hydrophobic fields, i.e., models 14 and 15, showed good predictive ability. Model 15 resulted from the exclusion of lamellarin Y with the lowest cytotoxic activity in the training set for model 14, giving rise to a significantly increased r^2_{cv} value, even though the conventional r^2 and $r^2_{test\ set}$ values for both models were not significantly different. Thus, model 15 was chosen as the best CoMSIA model for the MDA-MB-231 cell line. The contributions from steric, electrostatic, and hydrophobic interactions were determined to be 10.2%, 49.9%, and 39.8%, respectively, similar to the values obtained from the CoMSIA model 8 for the T47D cell line.

The correlations between the actual $-\log IC_{50}$ data of lamellarins against the MDA-MB-231 cell line and the values predicted based on CoMFA model 5 and CoMSIA model 15 are shown in Fig. 6a and b, respectively. In the case of CoMFA model 5 (Fig. 6a), lamellarin L was the only compound in the test set for which the predicted cytotoxicity deviated from the actual value by more than one log unit, and the exclusion of this compound significantly increased the $r^2_{test\ set}$, from 0.364 to 0.612. A similar degree of deviation was also observed for the $-\log IC_{50}$ value of lamellarin α predicted using CoMSIA model 15 (Fig. 6b). Nevertheless, these results indicated that both CoMFA model 5 and CoMSIA model 15 could be used to predict the cytotoxicity of lamellarins towards the MDA-MB-231 cell line.

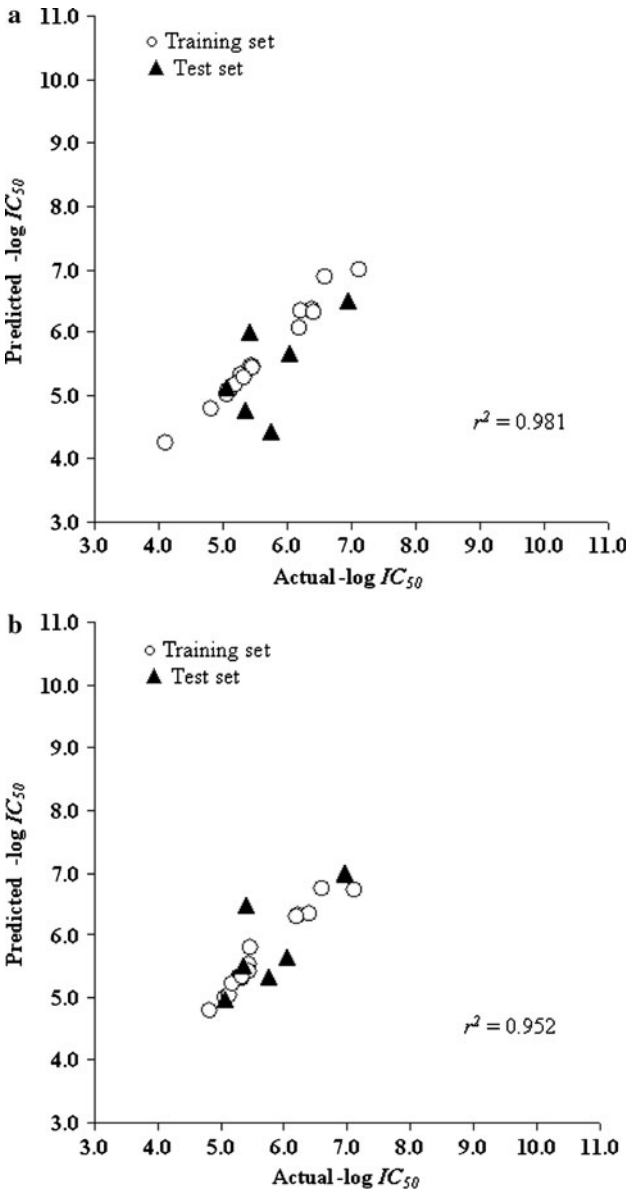

Fig. 6 Plot of the predicted versus actual cytotoxic activity of lamellarins against MDA-MB-231 cells. The predicted values were obtained from non-cross-validated CoMFA model 5 (**a**) and CoMSIA model 13 (**b**) for the compounds in both the training (*open circle*) and test (*filled triangle*) sets

CoMFA and CoMSIA contour maps

The steric and electrostatic maps of the CoMFA analysis for the MDA-MB-231 cell line are presented in Fig. 4b. Blue and green regions were found around hydroxy and methoxy groups at C9, and red regions located near the oxygen atom at C8 and C9. These might indicate that a steric electropositive group at C9 would increase cytotoxicity. However, there were only two lamellarins (Y and dehydrolamellarin Y) which have a hydroxyl group at C9. Hence, this might suggest only that the oxygen atom at C8

and C9 and an electropositive group at C9 would play an important role in increasing cytotoxic activity. The green, yellow, and blue contours near the hydroxyl group at C7 showed that the C7 area preferred a steric electropositive group, but it should not be too large. These results were supported by the experimental data reported in Tables 1 and 2. Lamellarins K, E, F, M, X, and ε with the hydroxyl group at C7 were more cytotoxic against MDA-MB-231 cell line than were lamellarins C, T, I, B, W, and ζ, respectively. Moreover, this result supports the conclusion of Chittchang et al. [27], as shown in the CoMSIA analysis for the T47D cell line. There was a yellow contour located behind the plane of the D-ring near the C5–C6 bond. This revealed the importance of a double bond at C5–C6 to enhance the MDA-MB-231 cytotoxic activity, similar to case of T47D activity. The red contours near the oxygen atom at C14 suggest that the oxygen atom at C14 would play an important role in increasing cytotoxic activity. The blue contour near C20 indicates that occupancy of an electropositive group at this position would help cytotoxic activity.

The steric, electrostatic, and hydrophobic contour maps of the CoMSIA model for the MDA-MB-231 cell line are displayed in Fig. 5b. Green and blue contours were found near C9. Additionally, a white region was found between C8 and the oxygen atom at C9. From these results it can be concluded that an electropositive group at C9 enhances cytotoxic activity. There were green contours between C7 and C8, yellow and blue contours at C7, and red contours around C7 and the C5–C6 bond. These suggest that a steric group disfavoring hydrophobic interactions at C8 is preferred. However, there were only two pairs of lamellarins for which direct comparison of the effect of substituting the hydroxyl group at C8 by a methoxy group could be made (lamellarin L compared with lamellarin U and lamellarin N compared with lamellarin α). Three of them (L, U, and α) were in the test set. At C7, a steric electron-donating oxygen-containing group which was not too large might be required to increase activity. Thus, the finding of CoMSIA analysis at C7 for the MDA-MB-231 cell line confirms the structure–activity relationship (SAR) result from the report of Chittchang et al. [27]. Both hydrophobic fields (white and orange contours) were found near the C5–C6 bond. The importance of an oxygen atom was also shown near the acetate group at C14 and C20 by red regions. The final contour is the green region at C21, representing the methoxyl group at this position.

Common structural requirement of lamellarins as a binding pocket of the T47D compared with the MDA-MB-231 cell lines

In summary, the T47D and MDA-MB-231 receptor binding site models are proposed as shown in Fig. 7a and b, respectively. By using the combination of CoMFA and CoMSIA results, the structural requirement of lamellarins at the binding pockets of both cell lines are shown by common carbon atoms of the lamellarin skeleton. Figure 7a reveals that the double bond at C5–C6, the electropositive groups at C9, C13, and C21, a nonsteric electropositive group at C8, and a steric electron-donating oxygen-containing group at C7 are required for cytotoxic activity. Based on Fig. 7, the 3D-QSAR analysis revealed that the common structure of lamellarins around the binding pocket for both cell lines was similar in many positions, e.g., at C7, C9, and the C5–C6 bond. More importantly, this method showed some different structural requirements of the lamellarin skeleton for both cell lines, such as a nonsteric electropositive group at C8 in case of T47D cells. For the MDA-MB-231 cell line, on the other hand, the C8 area seemed to require a steric group disfavoring hydrophobic interactions. Additionally, the electropositive groups at C13 and C21, which appear crucial in case of the T47D cell line, were not important for the MDA-MB-231 cell line. The presence of an electropositive group at C20 may be important in case of the MDA-MB-231 cell line, but such an inclusion did not show any significant cytotoxicity for the T47D cell line. The requirement of a steric group disfavoring hydrophobic interactions at C8 may account for the potent cytotoxic activity of lamellarins M,

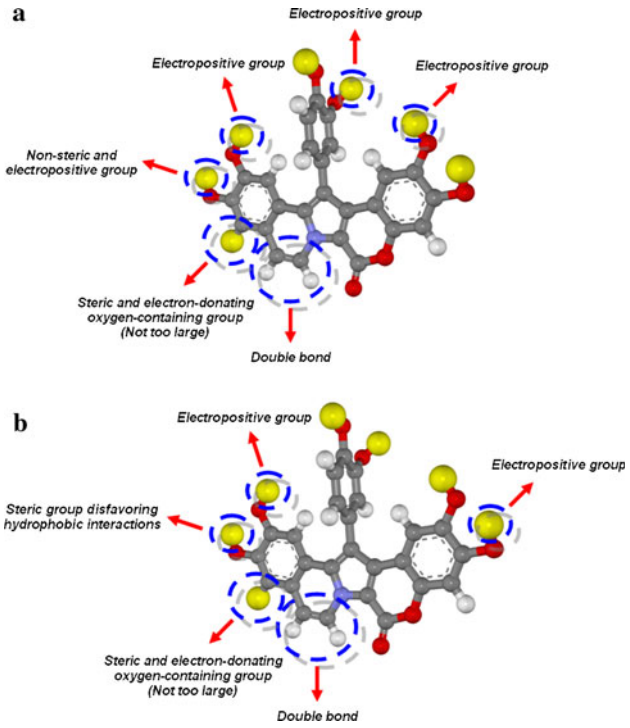

Fig. 7 Structural requirements of lamellarins for (**a**) T47D and (**b**) MDA-MB-231 receptor binding site obtained from combination of the CoMFA and CoMSIA contour maps

X, and ε against the MDA-MB-231 cell line, as shown in Table 2.

The importance of the substitution on F- and E-rings of lamellarin has been discussed in 4D-QSAR analysis using the same data set [28]. Overall, 4D-QSAR models found that the formation of an intermolecular hydrogen bond and the hydrophobic interactions for substituents on the E-ring most strongly modulated cytotoxicity towards T47D. Especially the 3D pharmacophore site near C8 and C9 from the 4D-QSAR model of a high-activity data set is seemingly distinguished from the 4D-QSAR model of the overall data set. A hydrophobic substituent on the F-ring can also increase cytotoxicity against the T47D cell line. 3D-QSAR analysis can also reveal some interesting structural requirements of lamellarins at C7, C8, C9, and C13, as shown in Fig. 7a. However, previous 4D-QSAR analysis cannot depict the different cytotoxicity of lamellarins containing saturated and unsaturated D-rings. The yellow contour near the C5–C6 double bond confirms that the binding pocket site prefers the unsaturated D-ring lamellarins over saturated D-ring lamellarins.

Conclusions

The 3D-QSAR methods CoMFA and CoMSIA were applied to lamellarins for cytotoxicity against T47D and MDA-MB-231 breast cancer cells. Lamellarins with saturated and unsaturated D-rings which bear different planarity at D- and E-ring structures were the focus. Satisfactory CoMFA and CoMSIA models were derived, and the obtained results revealed that these powerful 3D-QSAR methods can be used to handle even small data sets consisting of two groups of different types of geometries. As there is no information about the target structure for both cell lines, CoMFA and CoMSIA analyses provided more details about the steric, electrostatic, and hydrophobic field requirements of lamellarins for breast cancer cytotoxicity. In addition, the CoMSIA contour maps showed good correlation with those obtained by CoMFA. Based on CoMFA and CoMSIA contour maps, the results can discriminate the structural requirements between T47D and MDA-MB-231 cytotoxicity by common carbon atoms of the lamellarin skeleton such as at C8, C13, C20, and C21. Interestingly, different structural requirements of lamellarins at C8 may play an important role in the different cytotoxicity against the two cell lines. In the T47D cell line, 3D-QSAR contours highlight the importance of the F-ring at C13 for cytotoxicity; on the other hand, this did not occur in contour maps around this region for the MDA-MB-231 cell line. The contour maps of both cell lines suggest the necessity of the A-ring at C21 for cytotoxicity against the T47D cell line, but the importance of the A-ring for cytotoxicity against the MDA-MB-231 cell line is clearly shown at C20.

Moreover, the 3D-QSAR results revealed specific structural requirements of the lamellarins for their cytotoxic activity towards two breast cancer cell lines, including a steric electropositive oxygen-containing group at C7, and an electropositive group at C9. Especially, the significance of the C5–C6 double bond was also found. Hence, 3D-QSAR is a useful method to explore the specific structural requirements between both types of human breast cancer cells and also as a guideline to design more effective inhibitors from lamellarins. These are not only helpful for more detailed understanding of the interactions of lamellarin derivatives upon binding to an unknown receptor, but are also applicable to a small lamellarin data set.

Methods

Lamellarin compounds and cytotoxicity assays

The 26 lamellarins used in this study (Tables 1, 2) were synthesized and purified as described previously [29]. All compounds were solubilized in dimethyl sulfoxide (DMSO) and tested for their cytotoxic activity against T47D and MDA-MB-231 cell lines as previously reported [27]. Briefly, the cells were incubated in 96-well microplates at 37 °C for 48 h with serial dilutions of the test compounds, positive control (etoposide), or negative control (DMSO). The number of surviving cells in each well was determined using crystal violet staining to obtain the IC_{50} value, defined as the concentration that inhibits cell growth by 50% after 48 h of continuous exposure to each test compound. The values thus obtained were then transformed by calculating their negative logarithm (i.e., $-\log IC_{50}$), which is a standard notation to make very small numbers fit into a more comprehensible range; larger values indicate more potent cytotoxicity.

Alignment rules, CoMFA and CoMSIA calculations

Lamellarin molecules were separated into two groups. The first group, consisting of 20 compounds, served as the training set. On the other hand, six compounds comprising the test set were chosen at random to include structurally diverse molecules possessing a wide range of cytotoxic activity against both cell lines, namely lamellarins α, K, L, M, T, and U. The starting geometries of all 26 lamellarin structures were fully optimized at the HF/3-21G level using the GAUSSIAN 03 program [33]. The partial atomic charges required for calculations of electrostatic interactions were subsequently computed using the Gasteiger-

Hückel method in the SYBYL 7.0 program (Tripos, L.P., St. Louis, MO, USA). Molecular alignments were then carried out using the matching method also available in the SYBYL software. The common structure used for matching alignments involves the atoms constituting the A-, B-, and C-rings, as denoted with asterisks in Fig. 1. Additionally, the most active molecule with respect to each cell line, i.e., lamellarin D for T47D and lamellarin X for MDA-MB-231 cells, was used as the template for alignments.

To calculate the CoMFA and CoMSIA descriptor fields, a cubic lattice was first generated around each lamellarin molecule based on its molecular volume, and a grid spacing of 2 Å was used to ensure that the grid extended by 4.0 Å beyond the molecular dimensions in all directions. In addition to an sp^3 carbon atom with a +1 charge, which is the default probe atom in SYBYL, an sp^3 oxygen atom with a −1 charge and a hydrogen atom with a +1 charge were also used as additional probe atoms for CoMFA calculations in this study, and these atoms were placed at each lattice point. On the other hand, the steric and electrostatic fields of each aligned lamellarin were generated based on their Lennard–Jones and Coulomb potentials, respectively. The interactions between these three-dimensional fields with each probe atom were then calculated using the CoMFA standard scaling technique, in which the minimum sigma value was set at 8.4 kJ/mol, and an energy cutoff value of 125 kJ/mol was selected to not only speed up the analysis but also reduce the amount of noise. All the calculated data were then put into a CoMFA table.

In CoMSIA, five similarity indices (including steric, electrostatic, hydrophobic, H-bond donor, and H-bond acceptor descriptors) were computed for each lamellarin molecule using the same cubic lattice employed for the CoMFA calculations, as well as the default carbon probe atom with 1 Å radius and +1 charge. The hydrophobic, H-bond donor, and H-bond acceptor fields were established more than generally potentials (Lennard–Jones and Coulomb) in CoMFA analysis. The relative contributions of the different fields were generated during this analysis. The three-dimensional properties of lamellarins determined using either CoMFA or CoMSIA were then correlated with their cytotoxic activity against each cell line using partial least-squares (PLS) regression analysis, and various 3D-QSAR models were subsequently derived.

The predictive ability of the derived 3D-QSAR models was evaluated by leave-one-out (LOO) cross-validation, and is expressed in terms of r^2_{cv} (also called q^2), which is defined as shown in Eq. 1.

$$r^2_{cv} = (SSY - PRESS)/SSY, \quad (1)$$

where SSY represents the variance of the cytotoxic activity of molecules around the mean value, and PRESS is the prediction error sum of squares derived from the leave-one-out method. In contrast, the uncertainty of the prediction (S-PRESS) is defined as shown in Eq. 2.

$$S\text{-}PRESS = [PRESS/(n-k-1)]^{1/2}, \quad (2)$$

where n is the number of compounds used in the study, and k is the number of PLS components.

For all models, a maximum number of components was first used and subsequently decreased until an optimal number was obtained when the resulting cross-validated r^2_{cv} differed from the previous value by <0.05. The optimal number of components was then used to perform non-cross-validated analyses. Briefly, the conventional correlation coefficient, r^2, was calculated based on the 20 compounds in the training set. The CoMFA and CoMSIA models with r^2 value higher than 0.6 were subsequently validated by evaluating the correlations between the observed and predicted cytotoxic activities of the compounds in the test set, as indicated by the $r^2_{test\ set}$ values.

Acknowledgments This work would not have been possible without generous support from the Chulabhorn Research Institute (CRI), the Chulabhorn Graduate Institute (CGI), Phetchaburi Rajabhat University (PBRU), the Kasetsart University (KU) Graduate School, and the Commission on Higher Education (CHE). The Thailand Research Fund (TRF) is gratefully acknowledged for research grants (RTA5080005 to S.H., BRG5180013 to P.P., RMU4980048 to N.T., and DBG5180015 to M.C.). Moreover, the authors would like to thank the National Center of Excellence in Petroleum, Petrochemicals, and Advanced Materials, KU Research and Development Institute (KURDI), Laboratory for Computational and Applied Chemistry (LCAC) and the computing centre of KU, the Center of Nanotechnology KU, NANOTEC Center of Excellence at KU, and the Large Scale Research Laboratory of the National Electronics and Computer Technology (NECTEC) for computing and research facilities.

References

1. Andersen RJ, Faulkner DJ, He CH, Van Duyne GD, Clardy J (1985) J Am Chem Soc 107:5492
2. Carroll AR, Bowden BF, Coll JC (1993) Aust J Chem 46:489
3. Davis RA, Carroll AR, Pierens GK, Quinn RJ (1999) J Nat Prod 62:419
4. Ham J, Kang H (2002) Bull Korean Chem Soc 23:163
5. Krishnaiah P, Reddy VLN, Venkataramana G, Ravinder K, Srinivasulu M, Raju TV, Ravikumar K, Chandrasekar D, Ramakrishna S, Venkateswarlu Y (2004) J Nat Prod 67:1168
6. Lindquist N, Fenical W, Van Duyne GD, Clardy J (1988) J Org Chem 53:4570
7. Reddy MVR, Faulkner DJ, Venkateswarlu Y, Rao MR (1997) Tetrahedron 53:3457
8. Reddy SM, Srinivasulu M, Satyanarayana N, Kondapi AK, Venkateswarlu Y (2005) Tetrahedron 61:9242
9. Urban S, Butler MS, Capon RJ (1994) Aust J Chem 47:1919
10. Urban S, Capon RJ (1996) Aust J Chem 49:711
11. Urban S, Hobbs L, Hooper JNA, Capon RJ (1995) Aust J Chem 48:1491
12. Reddy MVR, Rao MR, Rhodes D, Hansen MST, Rubins K, Bushman FD, Venkateswarlu Y, Faulkner DJ (1999) J Med Chem 42:901

13. Ridley CP, Reddy MVR, Rocha G, Bushman FD, Faulkner DJ (2002) Bioorg Med Chem 10:3285
14. Fan H, Peng J, Hamann MT, Hu JF (2008) Chem Rev 108:264
15. Facompre M, Tardy C, Bal-Mahieu C, Colson P, Perez C, Manzanares I, Cuevas C, Bailly C (2003) Cancer Res 63:7392
16. Vanhuyse M, Kluza J, Tardy C, Otero G, Cuevas C, Bailly C, Lansiaux A (2005) Cancer Lett 221:165
17. Costantini P, Jacotot E, Decaudin D, Kroemer G (2000) J Natl Cancer Inst 92:1042
18. Debatin KM, Poncet D, Kroemer G (2002) Oncogene 21:8786
19. Dias N, Bailly C (2005) Biochem Pharmacol 70:1
20. Kluza J, Gallego MA, Loyens A, Beauvillain JC, Sousa-Faro JMF, Cuevas C, Marchetti P, Bailly C (2006) Cancer Res 66:3177
21. Mayer AMS, Gustafson KR (2008) Eur J Cancer 44:2357
22. Baunbaek D, Trinkler N, Ferandin Y, Lozach O, Ploypradith P, Rucirawat S, Ishibashi F, Iwao M, Meijer L (2008) Mar Drugs 6:514
23. Quesada AR, Garcia Gravalos MD, Fernandez Puentes JL (1996) Br J Cancer 74:677
24. Bailly C (2004) Curr Med Chem Anticancer Agents 4:363
25. Ishibashi F, Tanabe S, Oda T, Iwao M (2002) J Nat Prod 65:500
26. Marco E, Laine W, Tardy C, Lansiaux A, Iwao M, Ishibashi F, Bailly C, Gago F (2005) J Med Chem 48:3796
27. Chittchang M, Batsomboon P, Ruchirawat S, Ploypradith P (2009) ChemMedChem 4:457
28. Thipnate P, Liu J, Hannongua S, Hopfinger AJ (2009) J Chem Inf Model 49:2312
29. Ploypradith P, Petchmanee T, Sahakitpichan P, Litvinas ND, Ruchirawat S (2006) J Org Chem 71:9440
30. Bohm M, Sturzebecher J, Klebe G (1999) J Med Chem 42:458
31. Cramer RD III, Patterson DE, Bunce JD (1988) J Am Chem Soc 110:5959
32. Klebe G, Abraham U, Mietzner T (1994) J Med Chem 37:4130
33. Frisch MJ, Trucks GW, Schlegel HB, Scuseria GE, Robb MA, Cheeseman JR, Montgomery JA Jr, Vreven T, Kudin KN, Burant JC, Millam JM, Iyengar SS, Tomasi J, Barone V, Mennucci B, Cossi M, Scalmani G, Rega N, Petersson GA, Nakatsuji H, Hada M, Ehara M, Toyota K, Fukuda R, Hasegawa J, Ishida M, Nakajima T, Honda Y, Kitao O, Nakai H, Klene M, Li X, Knox JE, Hratchian HP, Cross JB, Bakken V, Adamo C, Jaramillo J, Gomperts R, Stratmann RE, Yazyev O, Austin AJ, Cammi R, Pomelli C, Ochterski JW, Ayala PY, Morokuma K, Voth GA, Salvador P, Dannenberg JJ, Zakrzewski VG, Dapprich S, Daniels AD, Strain MC, Farkas O, Malick DK, Rabuck AD, Raghavachari K, Foresman JB, Ortiz JV, Cui Q, Baboul AG, Clifford S, Cioslowski J, Stefanov BB, Liu G, Liashenko A, Piskorz P, Komaromi I, Martin RL, Fox DJ, Keith T, Al-Laham MA, Peng CY, Nanayakkara A, Challacombe M, Gill PMW, Johnson B, Chen W, Wong MW, Gonzalez C, Pople JA (2004) Gaussian 03. Gaussian Inc., Wallingford